Supplement of Nat. Hazards Earth Syst. Sci., 26, 5691–5710, 2026
https://doi.org/10.5194/nhess-26-5691-2026-supplement
© Author(s) 2026. CC BY 4.0 License.



Natural Hazards and Earth System Sciences
Open Access
EGU

Supplement of

21st-century strong wind and heavy precipitation hazards in the Asian monsoon region related to mesoscale convective systems: climatology, variability, and trends

Jie Feng et al.

Correspondence to: Zhongdong Duan (duanzd@hit.edu.cn)

The copyright of individual parts of the supplement might differ from the article licence.

Supplement

This Supplement presents additional information, sensitivity analyses, and supporting results that complement the main text. The supplementary figures and tables are numbered according to their order of citation in the main text.

1 Sensitivity analysis of MCS identification thresholds

This study conducted additional threshold sensitivity tests to assess the robustness of the main results to parameter selection. Considering the computational cost of MCS identification and tracking over a large domain and long time period, the analysis was limited to the ECAS region for 2001–2023. Specifically, we performed MCS identification and tracking over the region 110°–127°E, 25°–42°N, which is slightly larger than the ECAS domain (112°–125°E, 27°–40°N). A one-at-a-time sensitivity analysis was then carried out, in which only one threshold was varied in each test while the remaining thresholds were fixed at their reference values. The reference thresholds were set to a CCS threshold of 225 K, a duration threshold of 3 h, an overlap ratio threshold of 0.15, and an area threshold of 3000 km², consistent with those used in the manuscript. The tested parameter values included CCS thresholds of 220 and 230 K, duration thresholds of 2 and 4 h, overlap ratio thresholds of 0.10 and 0.20, and area thresholds of 2000 and 4000 km². For each threshold setting, the interannual trends of selected metrics, including MCSD and MCSH, were calculated over the ECAS region to evaluate the sensitivity of the results to threshold selection.

For the cold-cloud threshold (233 K), this study did not conduct an additional sensitivity analysis of the same type, primarily because the identification of cold-cloud systems is relatively insensitive to changes in this threshold. As shown in Fig. 3b, the number of identified cold-cloud systems remains nearly unchanged across the 230–245 K threshold range.

Figure S2 compares the normalized interannual trends of four representative metrics under different threshold perturbations, where the normalized trend is defined as the ratio of the interannual trend to the corresponding multi-year mean over 2001–2023. The results show that the CCS threshold and the duration threshold have relatively larger impacts on the results, particularly on the normalized interannual trends of MCSD and MCSP. Moreover, these results appear to suggest that MCSs with more active convective characteristics (i.e., lower cloud-top temperatures) and longer durations tend to exhibit larger upward trends in their precipitation impacts, as illustrated in Fig. S2a, S2b. Figure S3 further summarizes the sensitivity of the normalized interannual trends of all key metrics to threshold selection. Although the trend values differ across threshold settings, all metrics retain upward trends, supporting the robustness of the main conclusions of this study to threshold selection.

Tables S1 and S2 further list the trend values and normalized trends of the key metrics in the manuscript under different threshold settings. The main differences arise in a few specific threshold settings, under which the interannual trends of some metrics do not reach statistical significance at the 5% level based on a two-tailed Student's t-test. For example, under the

threshold combination of a CCS threshold of 230 K, an overlap ratio threshold of 0.15, a duration threshold of 3 h, and an area threshold of 3000 km², the interannual trend of MCSH is not significant at the 5% level.

It should be noted that, to ensure comparability among the threshold sensitivity experiments, the supplementary analysis was conducted using the same identification domain and statistical window settings across all tests. Therefore, even though the reference-threshold experiment used the same threshold parameters as the main analysis in the manuscript, the corresponding results from the present sensitivity analysis differ slightly from those reported in the manuscript. This difference mainly arises from the adjustment of the identification domain rather than from changes in the thresholds themselves, and therefore does not affect the overall conclusions of the threshold sensitivity assessment.

2 Assessment of uncertainty associated with temporal matching scale

To further assess the potential influence of the uncertainty associated with daily-scale matching, this study conducted supplementary analyses for heavy rainfall events (HREs) and strong wind events (SWEs), respectively. For HREs, we redefined and recalculated MCS-HREs based on half-hourly MCS precipitation (MCSP). Specifically, we first accumulated half-hourly MCSP to obtain the daily MCS-related precipitation, and defined cases with daily accumulated MCSP ≥ 50 mm as MCS-HREs. This study then further analysed the MCS-HRE fraction and the interannual trend in MCS-HRE frequency. The results (Fig. S6) show that the daily-scale method used in the manuscript does indeed overestimate the MCS-HRE fraction to some extent. Nevertheless, the spatial patterns of the MCS-HRE fraction and the interannual trend in MCS-HRE frequency derived from the two methods are generally consistent. For the ECAS, the MCSP-based trend in MCS-HRE frequency is 0.080 d yr^{-1} (5.04% yr^{-1}), compared with 0.097 d yr^{-1} (3.79% yr^{-1}) obtained using the daily-scale method. Both trends pass the two-tailed Student's t-tests at the 95% confidence level.

For MCS-SWEs, this study used the hourly station observations available for 2016–2022 to calculate the MCS-SWE fraction during this period using both the daily-scale method described in the manuscript and the hourly-scale method. In the hourly-scale method, the unit of analysis remains a station day: for a station day with an observed SWE, if the station was covered by the MCS impact area within ±1 h of the SWE observation time, this station day was identified as an hourly-scale MCS-SWE. The results (Fig. S7) show that the daily-scale method results in a higher estimate of the MCS-SWE fraction than the hourly-scale method: under the daily-scale method, 46.7% of SWEs were identified as MCS-related events, whereas this fraction decreased to 32.8% under the stricter hourly-scale method. This difference is reasonable because the daily-scale method only requires an SWE to occur on a day with MCS activity and therefore applies a relatively loose temporal constraint, whereas the hourly-scale method requires MCS influence near the SWE observation time and thus imposes a stricter temporal constraint on the correspondence between SWE occurrence and MCS influence. Meanwhile, although the daily-scale method overestimates the magnitude of the MCS-SWE fraction, the spatial distribution patterns derived from the two methods remain broadly consistent, which indicates that the temporal matching scale mainly affects the estimated magnitude of the MCS-SWE fraction rather than its primary spatial distribution characteristics.

Therefore, we believe that this difference in temporal scale mainly affects the precise event-level correspondence between hazard occurrence and MCS activity, but does not materially affect the overall conclusions of this study regarding the regional and climatological statistical relationship between MCS activity and severe convective hazards.

3 Comparison with a previous MCS database

Figure S4 compares the distribution of MCSH between the MCS database developed in this study and that of Dong et al. (2022). The database of Dong et al. (2022) focuses on MCSs over mainland China, as indicated by the zero MCSH values over the ocean. Over land, the two datasets show broadly consistent MCSH patterns, with the main discrepancies in the eastern Tibetan Plateau, which we attribute to differences in the identification windows used in the two studies.

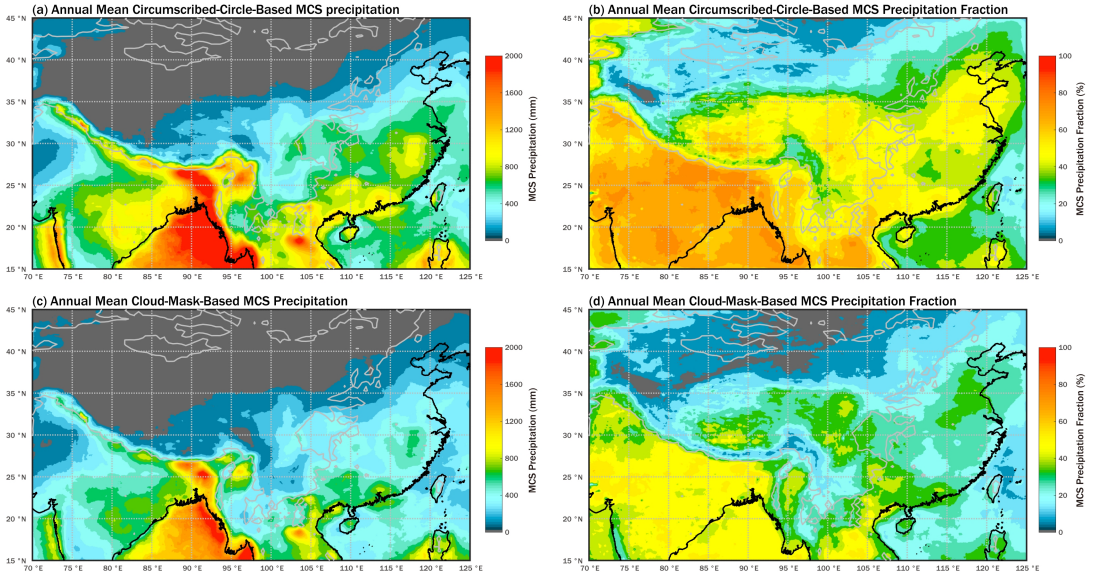


Figure S1: Annual mean spatial distributions of (a) circumscribed-circle-based MCS precipitation, (b) circumscribed-circle-based MCS precipitation fraction, (c) cloud-mask-based MCS precipitation, (d) cloud-mask-based MCS precipitation fraction. The black solid line represents the coastline, and the gray solid line represents the 1000 m elevation contour. Color shading indicates: annual mean (a, c) cumulative MCS precipitation (mm) and (b, d) MCS precipitation fraction (%).

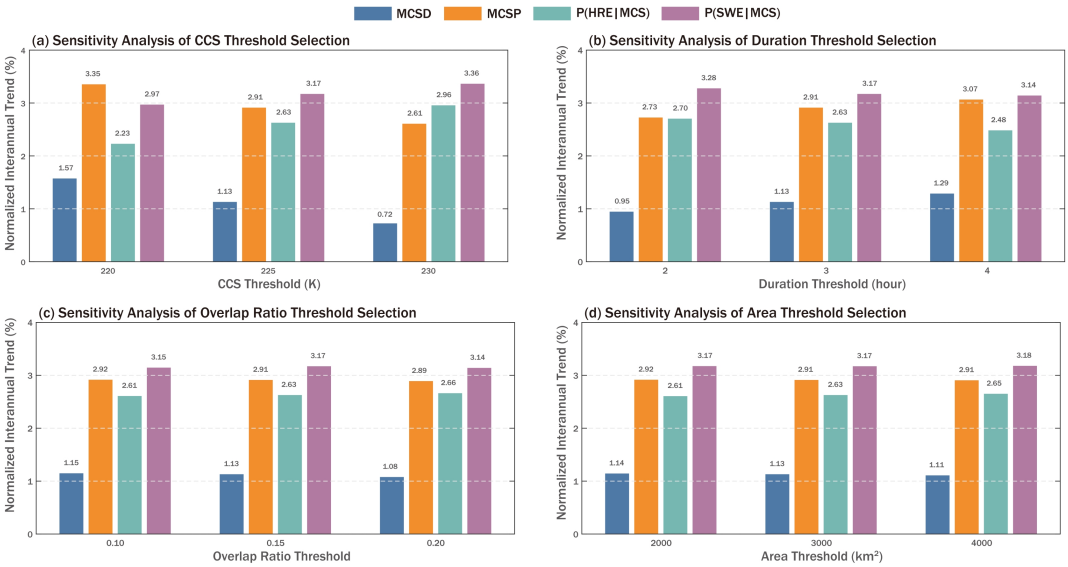


Figure S2: Sensitivity of the normalized interannual trends of MCSD, MCSP, P(HRE|MCS) and P(SWE|MCS) to (a) CCS threshold, (b) Duration threshold, (c) Overlap-ratio threshold, (d) Area threshold. All displayed trends are significant at the 5% level according to a two-tailed Student's t-test.

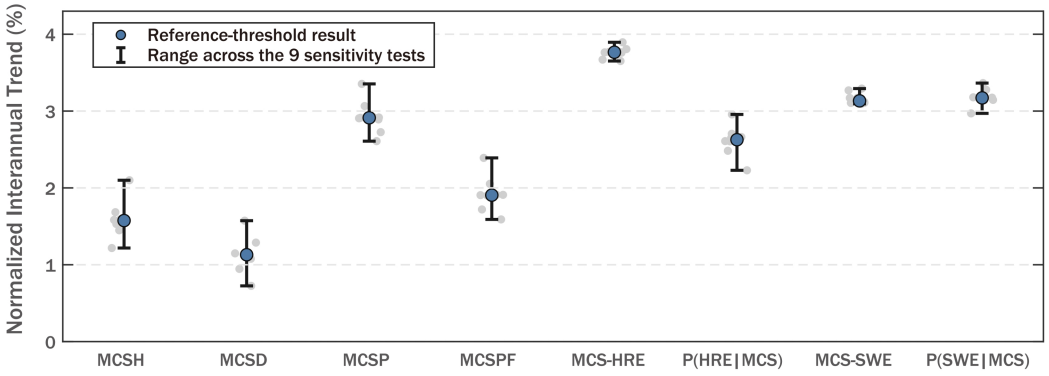


Figure S3: Sensitivity of key metrics to threshold perturbations. Gray dots represent the individual values obtained from the 9 tests. The reference-threshold results are obtained using a CCS threshold of 225 K, an overlap ratio threshold of 0.15, a duration threshold of 3 h, and an area threshold of 3000 km². Error bars indicate the minimum-to-maximum range across the 9 sensitivity tests.

75

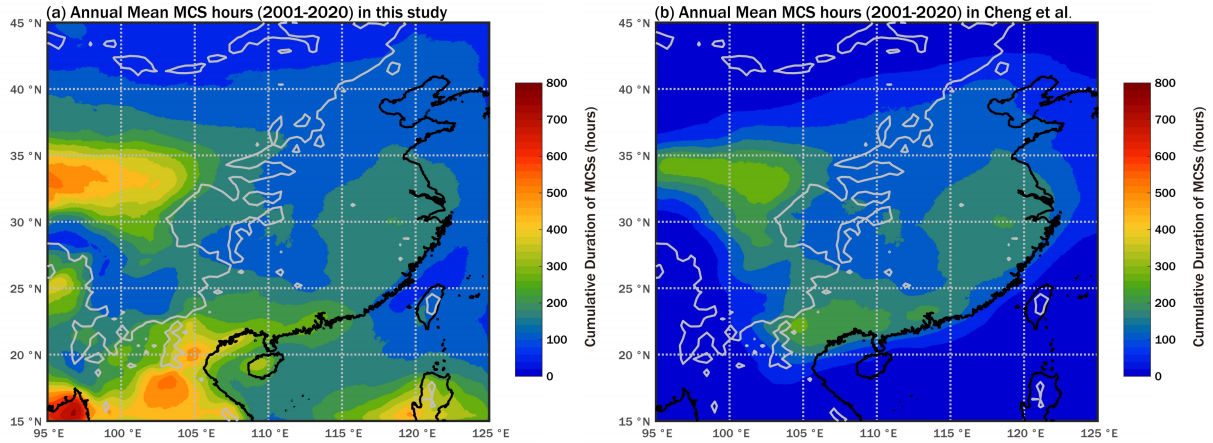


Figure S4: Annual mean spatial distributions of MCSH in (a) this study, (b) the study of Cheng et al. The black solid line represents the coastline, and the gray solid line represents the 1000 m elevation contour. Color shading indicates annual mean cumulative MCS duration.

Table S1: Interannual trends of MCSD, MCSH, MCSP, and MCSPF under different threshold settings. Values in parentheses denote the ratio of the trend to the corresponding multi-year mean. Underlined values indicate trends that are not statistically significant at the 5% level according to a two-tailed Student's t-test.

CCS threshold (K)	Overlap ratio threshold	Duration threshold (h)	Area threshold (km^2)	MCSD ($d \cdot yr^{-1}$)	MCSH ($h \cdot yr^{-1}$)	MCSP ($mm \cdot yr^{-1}$)	MCSPF ($pp \cdot yr^{-1}$)
225	0.15	3	3000	1.20(1.13%)	2.54(1.57%)	15.27(2.91%)	0.83(1.91%)
220	0.15	3	3000	1.36(1.57%)	2.83(2.10%)	15.18(3.35%)	0.88(2.39%)
230	0.15	3	3000	0.83(0.72%)	2.08(1.22%)	14.31(2.61%)	0.73(1.59%)
225	0.15	2	3000	1.05(0.95%)	2.45(1.45%)	14.86(2.73%)	0.78(1.72%)
225	0.15	4	3000	1.30(1.29%)	2.59(1.68%)	15.42(3.07%)	0.85(2.05%)
225	0.10	3	3000	1.22(1.15%)	2.56(1.58%)	15.31(2.92%)	0.83(1.91%)
225	0.20	3	3000	1.12(1.08%)	2.43(1.53%)	14.99(2.89%)	0.80(1.87%)
225	0.15	3	2000	1.22(1.14%)	2.58(1.59%)	15.40(2.92%)	0.83(1.91%)
225	0.15	3	4000	1.17(1.11%)	2.49(1.56%)	15.11(2.91%)	0.82(1.90%)

Table S2: Interannual trends of MCS-HRE, P(HRE|MCS), MCS-SWE, and P(SWE|MCS) under different threshold settings. Values in parentheses denote the ratio of the trend to the corresponding multi-year mean. Underlined values indicate trends that are not statistically significant at the 5% level according to a two-tailed Student's t-test.

CCS threshold (K)	Overlap ratio threshold	Duration threshold (h)	Area threshold (km^2)	MCS-HRE ($d \cdot yr^{-1}$)	*P*(*HRE*|*MCS*) ($pp \cdot yr^{-1}$)	MCS-SWE ($mm \cdot yr^{-1}$)	*P*(*SWE*|*MCS*) ($pp \cdot yr^{-1}$)
225	0.15	3	3000	0.097(3.77%)	0.063(2.63%)	0.071(3.13%)	0.062(3.17%)
220	0.15	3	3000	0.096(3.90%)	0.062(2.23%)	<u>0.066(3.27%)</u>	0.061(2.97%)
230	0.15	3	3000	0.096(3.67%)	0.067(2.96%)	0.074(3.09%)	0.065(3.36%)
225	0.15	2	3000	0.096(3.65%)	0.063(2.70%)	0.073(3.11%)	0.063(3.28%)
225	0.15	4	3000	0.097(3.81%)	0.061(2.48%)	0.072(3.29%)	0.062(3.14%)
225	0.10	3	3000	0.097(3.77%)	0.062(2.61%)	0.071(3.11%)	0.061(3.15%)
225	0.20	3	3000	0.097(3.77%)	0.065(2.66%)	<u>0.071(3.17%)</u>	0.061(3.14%)
225	0.15	3	2000	0.097(3.76%)	0.062(2.61%)	0.072(3.17%)	0.062(3.17%)
225	0.15	3	4000	0.097(3.76%)	0.064(2.65%)	0.070(3.12%)	0.062(3.18%)

Table S3: Definitions of the MCS metrics used in this study.

Metrics	Definition	Unit
MCSH	The cumulative duration of MCSs at each grid point.	hour
MCSD	Number of MCS-affected days at each grid point.	day
MCSP	The total precipitation related to MCSs.	mm
MCSPF	The ratio of MCSP to the total precipitation.	%
MCS-HRE	Number of heavy rainfall events associated with MCSs	day
P(HRE|MCS)	The conditional probability of HRE occurrence given MCS occurrence	%
MCS-SWE	Number of strong wind events associated with MCSs	day
P(*SWE*|*MCS*)	the conditional probability of SWE occurrence given MCS occurrence	%

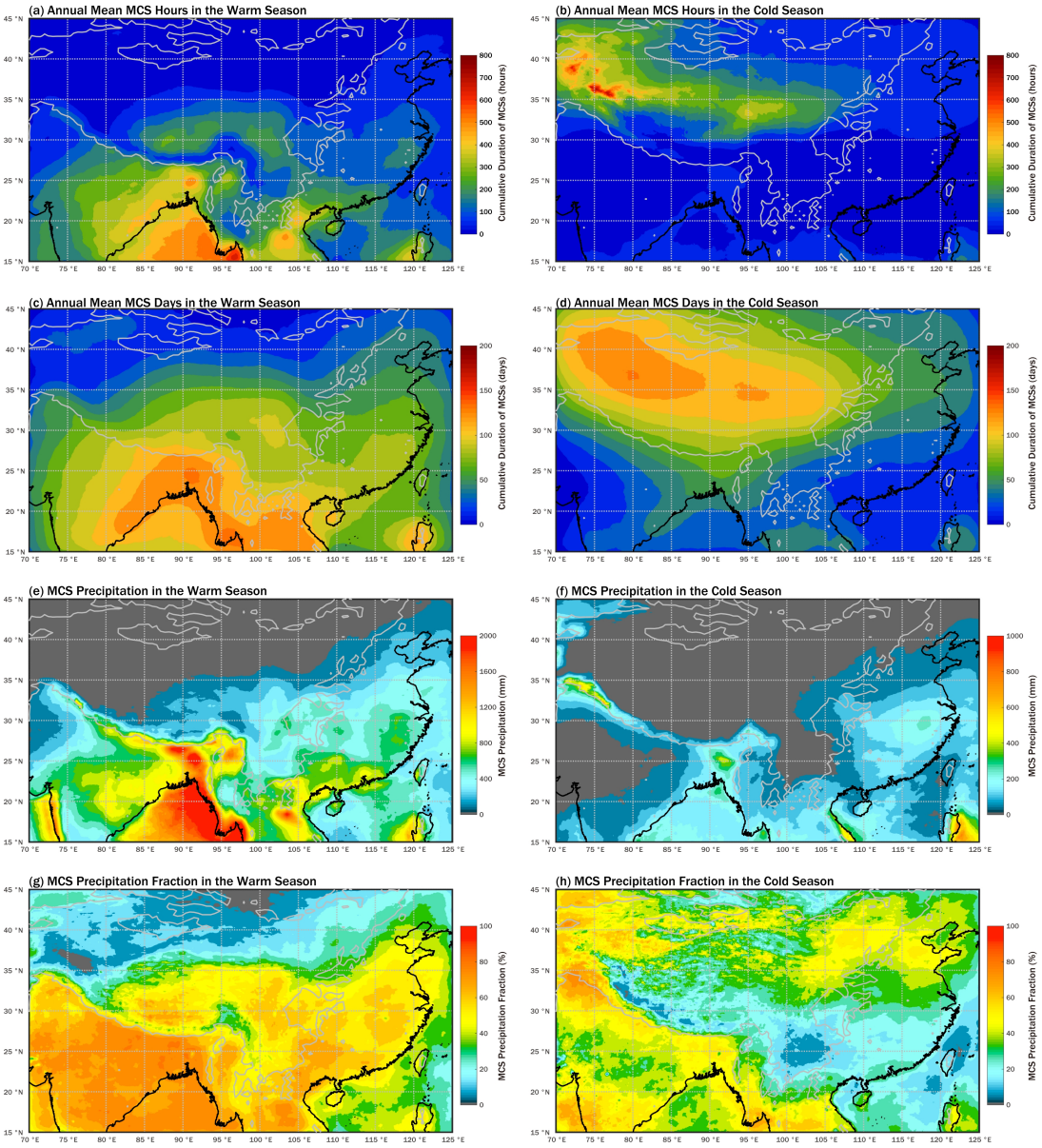


Figure S5: Annual mean spatial distributions of (a, b) MCSH, (c, d) MCSD, (e, f) MCSP, and (g, h) MCSPF, with warm-season results shown in the left column and cold-season results in the right column. The black solid line represents the coastline, and the gray solid line represents the 1000 m elevation contour. Color shading indicates: annual mean (a, b) cumulative MCS duration (hours), (c, d) number of MCS days (days), (e, f) cumulative MCS precipitation (mm), and (g, h) MCS precipitation fraction (%).

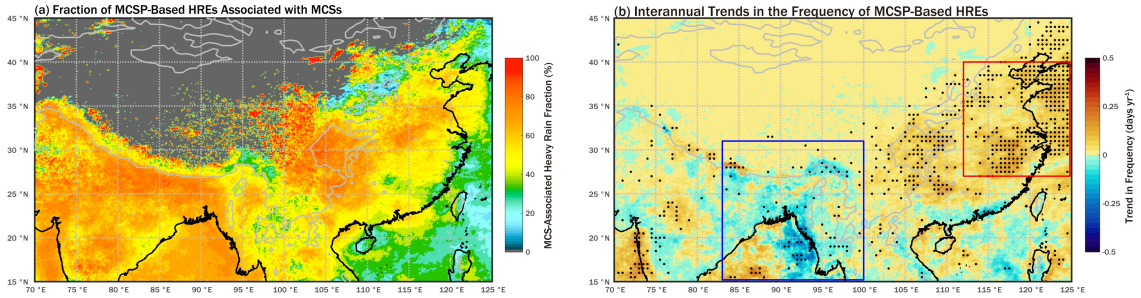


Figure S6: Spatial distribution of MCSP-based (a) MCS-HRE fraction, (b) interannual trend of MCS-HREs. The black solid line represents the coastline, and the gray solid line represents the 1000 m elevation contour. The color shading indicates the annual mean number of MCS-HRE fraction for (a) and annual trend of MCS-HREs (unit: d yr^{-1}) for (b). The black dots indicate regions with statistical significance at 5 % level, as determined by a two-tailed Student's t-test. The blue box indicates the range of BoBCR in this study, and the red box indicates the range of ECAS in this study.

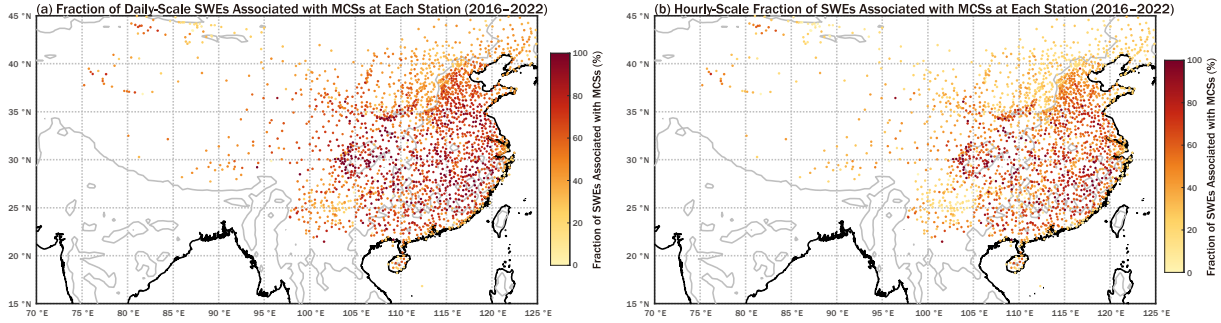


Figure S7: Spatial distribution of (a) daily-scale and (b) hourly-scale MCS-SWE fraction. The black solid line represents the coastline, and the gray solid line represents the 500 m elevation contour. The dots represent meteorological station locations. The color shading of dots indicates the number of MCS-SWE fraction.

105

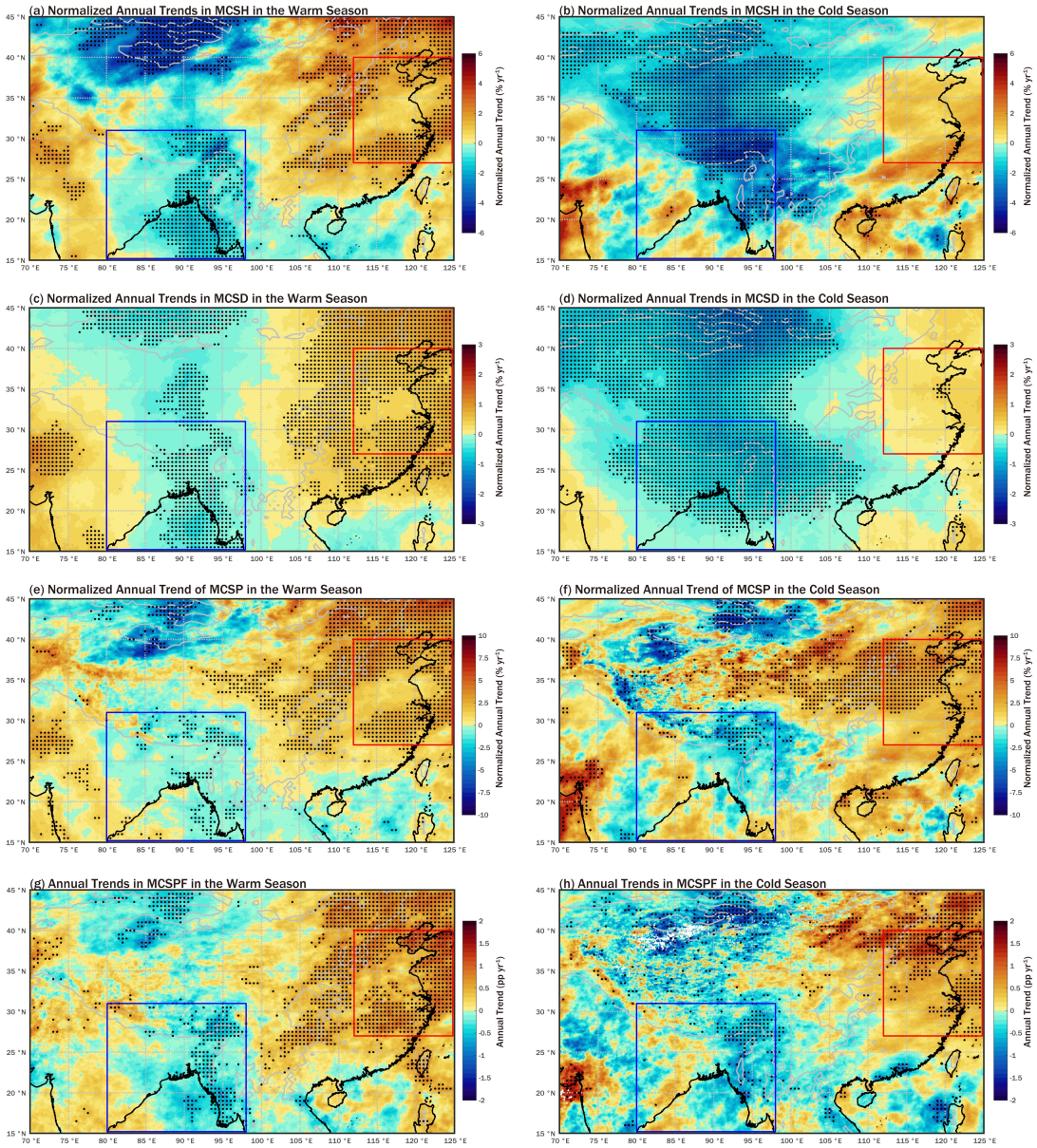


Figure S8: Spatial distribution of the interannual variations of (a, b) MCSH, (c, d) MCSD, (e, f) MCSP, and (g, h) MCSPF, with warm-season results shown in the left column and cold-season results in the right column. The black solid line represents the coastline, and the gray solid line represents the 1000 m elevation contour. The color shading in (a - f) denotes the normalized annual trend, which is the ratio of the interannual trend of each grid to its annual mean value (unit: % yr^{-1}); color shading in (g, h) denotes the annual trend (unit: % yr^{-1}). The black dots indicate regions with statistical significance at 5% level, as determined by a two-tailed Student's t-test. The blue box indicates the range of BoBCR in this study, and the red box indicates the range of ECAS in this study.